As evident upon examination of the data (Figure 2), **2** is comparable to **1** in volatility. The onset of weight loss (1 atm) for **1** is ~275 °C, changing slightly to ~300 °C for **2**. Data for **2** after sublimation and for commercially available[24] $Ba_5(tmhd)_9(OH)\cdot 3H_2O$ (**3**) also are presented for comparison. The reproducible shift to higher volatility (lower temperature weight loss) evidenced by **2** after sublimation is understood best by comparison of the IR data for it to those for **1**. Significant changes between 4000 and 2000 cm^{-1} in the IR spectra for **1**–**3** (Figure 3) are symptomatic of structural differences in these compounds. A broad absorption at ~3300–3200 cm^{-1} for **3** indicates the presence of O–H[25] in the compound. This absorption is not seen for **1**. For **2**, the N–H diagnostic absorption is evident at ~3200 cm^{-1}. The IR spectrum of **2** after sublimation is virtually identical to that of **1**. This indicates loss of coordinated ammonia upon sublimation of **2** (eq 1). However, other than the volatility and

$$\underset{\mathbf{1}}{4[Ba(tmhd)_2]_{3,4}} \underset{-28NH_3}{\overset{+28NH_3}{\rightleftharpoons}} \underset{\mathbf{2}}{7[Ba(tmhd)_2\cdot 2NH_3]_2} \qquad (1)$$

these differences in the IR spectra, **1**–**3** were spectroscopically remarkably similar (^1H and ^{13}C NMR). Therefore, to clearly differentiate between these compounds, we examined the solid-state structure of **2** by single-crystal X-ray diffraction.

Each Ba atom in **2** has local square-antiprismatic coordination. This results in a molecular symmetry of an axially enlongated cuboctahedron. The μ_2-oxygen atoms of the bridging tmhd ligands form the inside corners of this cube. The 45° skewed outside corners of the two cubes (vs the inside) are formed by two oxygen atoms of one terminal tmhd ligand and the nitrogen atoms of two ammonia ligands. One interesting feature of **2** is the somewhat shortened intramolecular Ba–Ba distance of 3.83 Å. To our knowledge, this is the lowest molecularity $Ba(acac)_2$-derived compound structurally characterized to date, and thus there are no other data available with which to directly compare the observed metal–metal distance in this dimeric species. We, and others, recently have observed interatomic distances between 4.03 and 4.12 Å for trimeric,[20a] pentameric,[24b] and hexameric[26] structures. The plane defined by a barium atom and its two ammonia ligands intersects the plane of the same barium atom and its two terminal oxygen atoms with an angle of 89.2°. The terminal tmhd ligands deviate by 15.5° from their normal planar configuration.[27] The bridging tmhd ligands intersect the Ba-$(\mu_2\text{-}O)_2$ planes with an angle of 130.4°.[28]

Compound **2** currently is undergoing evaluation as an OMCVD precursor in the fabrication of $YBa_2Cu_3O_{7-\delta}$ thin films on large-area (>2-in. diameter) substrates at low (<700 °C) deposition temperatures.[29] Initial results have been encouraging and will be reported in due course.

Acknowledgments. We gratefully acknowledge the generous financial support provided for this project from DARPA Contract No. MDA 972-88-J-1006 and the Deutsche Forschungsgemeinschaft (postdoctoral fellowship to W.H.). We also thank Professor Sievers for willingly sharing a preprint of ref 24b with us.

Supplementary Material Available: Tables of positional and thermal parameters and interatomic distances and angles for compound **2** and a textural presentation of the preparation and characterization data for compound **1** (10 pages); a listing of observed and calculated structure factors for compound **2** (19 pages). Ordering information is given on any current masthead page.

Department of Chemistry and Materials Research and Technology Center
The Florida State University
Tallahassee, Florida 32306-3006

William S. Rees, Jr.*
Michael W. Carris
Werner Hesse

Received June 19, 1991

(24) (a) Although supplied commercially as "anhydrous $Ba(tmhd)_2$", this frequently used OMCVD source material recently has been identified as $Ba_5(tmhd)_9(OH)\cdot 3H_2O$. (b) Turnipseed, S. B.; Barkley, R. M.; Sievers, R. E. *Inorg. Chem.* **1991**, *30*, 1164–1170. (c) The thermal instability of **3** at use temperatures (230–300 °C) is well documented. See ref 4 and references contained therein.
(25) Silverstein, R. M.; Bassler, G. C.; Morrill, T. C. *Spectrometric Identification of Organic Compounds*, 3rd ed.; Wiley: New York, 1974.
(26) Rees, W. S., Jr.; Carris, M. W.; Hesse, W.; Goedken, V. To be submitted for publication.
(27) (a) This angle is defined by the intersection of the plane containing Ba(01), O(03), and O(04) with the plane containing O(03), C(13), C(14), C(15), and O(04). (b) For a thorough compilation of structural data on metal acac complexes, see: Mehrotra, R. C.; Bohra, R.; Gaur, D. P. *Metal β-Diketonates and Allied Derivatives*; Academic: New York, 1978; pp 58–194.
(28) This angle is defined by the intersection of the plane containing Ba(01), O(01), and O(02) with the plane containing O(01), C(02), C(03), C(04), and O(02).
(29) Rees, W. S., Jr.; Stuckey, D.; Zhao, J.; Norris, P. E. To be submitted for publication.

An Interesting Low Barrier to Metal–Ligand Contrarotational Fluxionality in Closed 11-Vertex $[1,1\text{-}(PMe_2Ph)_2\text{-}1,2,3\text{-}PtC_2B_8H_9X]$ Compounds That Is Characterized by Arachno ⇌ Nido Geometric Changes within the 10-Vertex $\eta^6\text{-}\{C_2B_8H_9X\}$ Ligand[1]

There is a long and continuing fascination with the variations in the modes of interaction of transition-element centers with boron hydride and related clusters. This is exemplified classically by the ideas generated by the observation[2] in 12-vertex metalladicarbaborane compounds of the "slippage" from closed to open structures that arises from changes in the carbaborane-to-metal binding mode in the complexes of the 11-vertex η^5-{7,8-*nido*-$C_2B_9H_{11}$} ligand with platinum metals[3] and in the extension of these ideas to include a broader spectrum of metallic elements.[4] We here now report preliminary results of an interesting structural change in 11-vertex platinadicarbaborane chemistry.

The 11-vertex platinadicarbaborane $[1,1\text{-}(PPh_3)_2\text{-}1,2,3\text{-}PtC_2B_8H_{10}]$ (compound **1**) is known to exhibit a closed 11-vertex cluster structure with an η^6 cluster-to-metal interaction.[5,6] We have now found that its closely related PMe_2Ph congeners $[1,1\text{-}(PMe_2Ph)_2\text{-}1,2,3\text{-}PtC_2B_8H_9\text{-}2\text{-}X]$ (X = H, Me, Ph) also have a closely related closed cluster geometry, but in addition exhibit an interesting rotational fluxionality, *within the constraints of their closed η^6-carborane-to-metal bonding*, that is accompanied by a remarkable flexing of the 10-vertex $\eta^6\text{-}\{C_2B_8H_9X\}$ moiety between extreme nido and arachno 10-vertex geometries.

The solid-state molecular structures of $[1,1\text{-}(PPh_3)_2\text{-}1,2,3\text{-}PtC_2B_8H_{10}]$ (**1**)[5,6] and $[1,1\text{-}(PMe_2Ph)_2\text{-}2\text{-}Me\text{-}1,2,3\text{-}PtC_2B_8H_9]$ (**2**; upper diagram in Figure 1)[7] show orthogonally different rotational orientations of the $\{Pt(PR_3)_2\}$ moiety with respect to the $\{C_2B_8H_9X\}$

(1) Contribution No. 16 from the Leeds–Řež Anglo–Czech Polyhedral Collaboration (ACPC).
(2) Warren, L. F.; Hawthorne, M. F. *J. Am. Chem. Soc.* **1968**, *90*, 4823–4828.
(3) Mingos, D. M. P.; Forsyth, M. I.; Welch, A. J. *J. Chem. Soc., Chem. Commun.* **1977**, 605–607; *J. Chem. Soc., Dalton Trans.* **1978**, 1363–1374.
(4) Colquhoun, H. M.; Greenhough, T. J.; Wallbridge, M. G. H. *J. Chem. Soc., Chem. Commun.* **1977**, 737–738; *J. Chem. Soc., Dalton Trans.* **1979**, 619–628.
(5) Kukina, G. A.; Porai-Koshits, M. A.; Sergienko, V. C.; Štrouf, O.; Baše, K.; Zakharova, I. A.; Štíbr, B. *Izv. Akad. Nauk SSSR., Ser. Khim.* **1980**, 1686. Kukina, G. A.; Porai-Koshits, M. A.; Sergienko, V. C. *Koord. Khim.* **1986**, *12*, 561–570.
(6) Štíbr, B.; Janoušek, Z.; Baše, K.; Heřmánek, S.; Plešek, J.; Zakharova, I. A. *Collect. Czech. Chem. Commun.* **1984**, *46*, 1891–1894.
(7) Crystal Data for compound **2**:[9] $C_{19}H_{34}B_8P_2Pt$, M = 605.99, monoclinic, a = 947.6 (1) pm, b = 1547.7 (3) pm, c = 1804.0 (3) pm, β = 104.78 (1)°, V = 2.5581 (8) nm^3, Z = 4, space group $P2_1/n$, D_c = 1.57 Mg m^{-3}, μ = 53.82 cm^{-1}, $F(000)$ = 1184, R (R_w) = 0.0216 (0.0234) for refinement of 4200 unique absorption-corrected reflections with $I > 2.0\sigma(I)$ and $4.0 < 2\theta < 50.0°$.

0020-1669/91/1330-4481$02.50/0

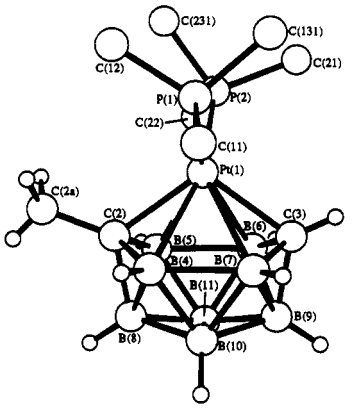

$[(PMe_2Ph)_2PtC_2B_9Me]$
(compound **2**)

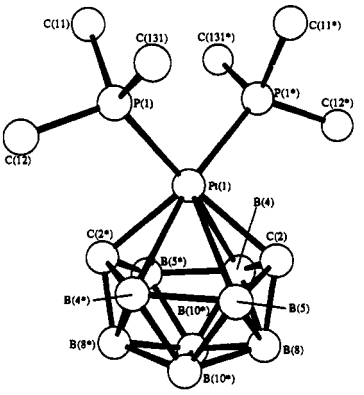

$[(PMe_2Ph)_2PtC_2B_8H_{10}]$
(compound **3**)

Figure 1. (Top) Drawing of the molecular structure of [1,1-$(PMe_2Ph)_2$-2-Me-1,2,3-$PtC_2B_8H_9$] (**2**). Selected interatomic distances (in pm) are as follows: from the platinum atom to P(1), 228.8 (3), to P(2), 228.8 (3), to C(2), 218.6 (6), to C(3), 217.6 (6), to B(4), 238.4 (7), to B(5), 237.7 (7), to B(6), 237.5 (7), and to B(7), 240.2 (7); from C(2) to C(2a), 152.0 (8), to B(4), 157.9 (9), to B(5), 156.8 (9); from C(3) to B(6), 156.7 (8), to B(7), 155.2 (9); from B(4) to B(7), 197.4 (9), and from B(5) to B(6), 198.8 (9). (Bottom) Drawing of the molecular structure of [1,1-$(PMe_2Ph)_2$-1,2,3-$PtC_2B_8H_{10}$] (**3**). Note that the molecule possesses a crystallographic C_2 axis passing through the platinum atom and midway between atoms B(10) and B(11). Selected interatomic distances (in pm) are as follows: from the platinum atom to P(1), 226.7 (4), to C(2), 215.5 (10), to B(4), 257.2 (13), and to B(5), 243.4 (13); from C(2) to B(4), 160.6 (16) and to B(5), 155.3 (17); from B(4) to B(5*), 189.6 (19).

(X = H, Me) dicarbaborane residue (Scheme I, structures **1** and **2**, respectively; see also the outer diagrams in Figure 2). The rotational orientation in the solid-state structure of [1,1-$(PMe_2Ph)_2$-1,2,3-$PtC_2B_8H_{10}$] (**3**; lower diagram in Figure 1)[8] is intermediate (structure **3** in Scheme I, and center diagram in Figure 2).

In compound **2** there is a prochirality of the *P*-methyl groupings, and use of $^1H\{^{31}P\}$ NMR spectroscopy on these at different temperatures[10,11] demonstrates that there is a rotational process in solution for this compound and also yields[12] an activation energy ΔG^*_{284} for the rotational process of 63 kJ mol^{-1}. The values of ΔG^* for the unsubstituted and thereby less sterically hindered PMe_2Ph species **3** must be much less than this, whereas their sterically more hindered 2-phenyl analogue [1,1-$(PMe_2Ph)_2$-2-Ph-1,2,3-$PtC_2B_8H_9$] (**4**) has a higher value (ΔG^*_{385} = 83 kJ mol^{-1}).[12] Consideration of the nature of the steric effects in **2** and **4** together with the similarity[13] of the cluster NMR char-

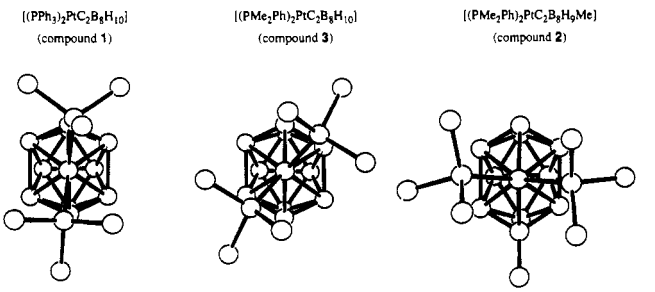

Figure 2. Drawings of (from left to right) the $\{P_2PtC_2B_8H_9X\}$ units of the crystallographically determined solid-state structures of compounds **1**, **3**, and **2**, respectively (X = H, Me, and H respectively), the view being chosen to illustrate the rotational twist. Data for compound **1** are taken from ref 5.

Scheme I

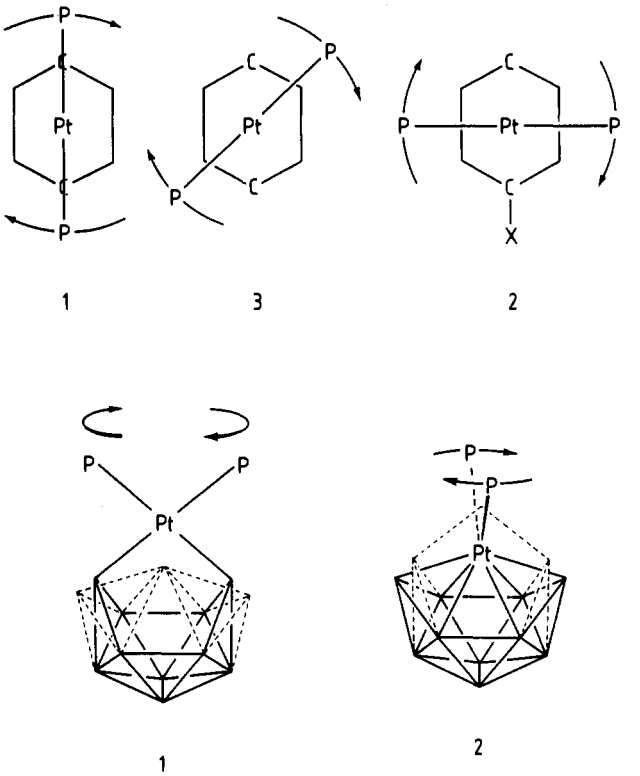

(8) Crystal data for compound **3**:[9] $C_{18}H_{32}B_8P_2Pt$, M = 591.69, monoclinic, a = 1824.8 (2) pm, b = 1016.8 (2) pm, c = 1328.2 (3) pm, β = 101.48 (2)°, V = 2.4150 (8) nm^3, Z = 4, space group $I2/a$ (=$C2/c$), D_c = 1.63 Mg m^{-3}, μ = 57.00 cm^{-1}, $F(000)$ = 1152, R (R_w) = 0.0442 (0.0474) for refinement of 2057 unique absorption-corrected reflections with $I > 2.0\sigma(I)$ and $4.0 < 2\theta < 50.0°$.

(9) All crystallographic measurements were made on a Nicolet P3/F diffractometer operating in the ω scan mode using graphite-monochromated X-ray radiation. The structures of both **2** and **3** were determined via standard heavy-atom methods and refined by full-matrix least-squares techniques. All non-hydrogen atoms for both complexes were refined with anisotropic thermal parameters. The phenyl and methyl hydrogen atoms of compound **2** were included in calculated positions and assigned to an overall isotropic thermal parameter. The borane hydrogen atoms of this compound were located in a Fourier difference synthesis and were refined with isotropic thermal parameters. Hydrogen atoms were not locatable for compound **3** but are apparent from the NMR analysis.[12,13] The weighting scheme $w = [\sigma^2(F_o) + 0.0004(F_o)^2]^{-1}$ was used for both compounds.

(10) Boocock, S. K.; Greenwood, N. N.; Kennedy, J. D. *J. Chem. Soc., Chem. Commun.* **1980**, 305–306. Boocock, S. K.; Greenwood, N. N.; Kennedy, J. D.; McDonald, W. S.; Staves, J. *J. Chem. Soc., Dalton Trans.* **1981**, 2573–2584.

(11) Ferguson, G.; Kennedy, J. D.; Fontaine, X. L. R.; Faridoon; Spalding, T. R. *J. Chem. Soc., Dalton Trans.* **1988**, 2555–2564.

(12) PMe_2Ph methyl group $\delta(^1H)$ NMR data for compounds **2**, **3**, and **4** as follows: compound **2** ($CD_3C_6D_5$ solution), +1.32 and +1.37 ppm at 271 K, coalescence temperature 284 K at 2.35 T (100 MHz), $\Delta\nu$(extrap) 7.4 Hz at 284 K; compound **3** (CD_2Cl_2 solution), +1.64 ppm at 294 K; compound **4** ($CD_3C_6D_5$ solution), +1.19 and +1.44 ppm at 294 K, coalescence temperature 385 K at 2.35 T (100 MHz), $\Delta\nu$(extrap) 22.4 Hz at 385 K.

Table I. Selected Interatomic Distances and Angles for the Platinadicarbaboranes **2**, **3**, and **1**, and for the Aluminadicarbaborane **6**

	2	**3**	**1**[a]	**6**[b]
C(2)···C(3)[c]	351.2 (6)	325.4 (14)	316.2 (13)	309.4
B(4)···B(5)[c]	257.0 (7)	268.7 (16)	265.0 (14)	265.3
B(6)···B(7)[c]	259.0 (7)	268.7 (16)	269.0 (15)	264.1
P(1)PtP(2)/C(2)C(3)[d]	85.2 (2)	48.9 (2)	6.2 (2)	87.9
Pt from C(2)C(3)[c]	129.3 (2)	141.3 (1)	145.4 (1)	131.1
C(2) from B(4)B(5)B(6)B(7)[c]	46.0 (4)	48.2 (9)	57.0 (8)	59.3
C(3) from B(4)B(5)B(6)B(7)[c]	44.0 (4)	48.2 (9)	62.1 (7)	59.1
C(2)–Pt–C(3)[d]	107.2 (3)	98.1 (3)	94.8 (3)	99.4

[a] Calculated from coordinates in ref 5. [b] Calculated from coordinates in ref 16; no esd's available; for Pt substitute Al and for the phosphines substitute $-OEt_2$ and ethyl. [c] In picometers. [d] In degrees.

acteristics in solution for all three PMe_2Ph compounds **2**–**4** show that configuration **2** (Scheme I) is the ground-state one for the molecules of all three of these species, including sterically unhindered **3**. The half-twist observed in the solid state for **3** (Scheme I and Figure 2) must therefore result from the balance of crystal packing forces versus the barrier to rotation in **3**, implying that this in this unhindered species is quite low (i.e. probably < ca 30 kJ mol^{-1}).

On the other hand, the mutually similar cluster NMR characteristics of the unsubstituted PPh_3 and SEt_2 analogues [1,1-$(PPh_3)_2$-1,2,3-$PtC_2B_8H_{10}$] (**1**) and [1,1-$(SEt_2)_2$-1,2,3-$PtC_2B_8H_{10}$] (**5**)[14] are markedly different from those of the PMe_2Ph compounds **2**–**4**. The two compounds **1** and **5** therefore have mutually similar cluster electronic structures that differ markedly from those of the three PMe_2Ph species. The solid-state structure of compound **1**[5,6] thence suggests that the alternative configuration **1** (Scheme I) is the ground-state one for these two species **1** and **5**. This would approximate to the maximum in the rotational barrier for the fluxional PMe_2Ph species **2**–**4**. There is at present no evidence for any fluxional behavior of compounds **1** and **5**, although we believe they may well be static.

Details of the solid-state structures of compounds **1**–**3** show that the rotational configurational differences are accompanied by marked changes in the geometry of the $\{PtC_2B_8\}$ cluster (Table I). For the PPh_3 compound **1** the platinum atom is much further out of the cluster (structure **1**, Scheme I), and the molecular structure has been interpreted[5] in terms of a square-planar platinum(II) moiety simply bridging the 6,9-positions[15] of the nido-type 10-vertex $\{6,9\text{-}C_2B_8H_{10}\}$ residue as is, for example, found in main-group analogues such as [$(OEt_2)EtAlC_2B_8H_{10}$] (**6**).[16] For the PMe_2Ph compound **2** the platinum atom is held much more compactly in the cluster (structure **2**, Scheme I), and it is now within much closer bonding distance of the four boron atoms. These differences are accompanied by a marked fundamental flexing of the 10-vertex $\{C_2B_8\}$ residue, manifested principally in a 35 (2) pm change in the C(2)···C(3) nonbonded distance between 316.2 (13) pm in **1** and 351.2 (6) pm in **2**. This we suggest

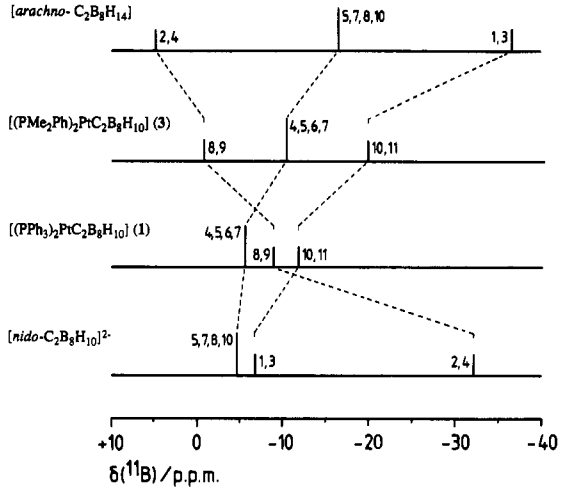

Figure 3. Stick representations of the chemical shifts and relative intensities in the ^{11}B NMR spectra of, successively from top to bottom, [*arachno*-6,9-$C_2B_8H_{14}$], compound **3**, compound **1**, and the [*nido*-6,9-$C_2B_8H_{10}]^{2-}$ anion. Hatched lines join equivalent positions for the four species.

corresponds to an extreme change from *nido*- to *arachno*-$\{C_2B_8\}$ 10-vertex geometrical character[17] (the corresponding difference between *nido*-$[B_{10}H_{14}]$ and *arachno*-$[B_{10}H_{14}]^{2-}$ being ca. 18 pm), which we believe in turn implies a greater orbital and electronic involvement of platinum with the cluster that could in some respects be interpreted as an effective increase in oxidation state from platinum(II) in **1** to platinum(IV) in **2** (compare refs 17 and 18). The half-twist distortions for the $\{C_2B_8H_{10}\}$ ligand in compound **3** are nicely intermediate in geometry, confirming that the derived solid-state structural differences between compounds **1** and **2** are not crystallographic artifacts.

These observations and considerations have a number of general implications in metallaborane and metallaheteroborane cluster chemistry, for example in the assessment of redox chemistry, in structural and bonding interpretations, and in the assessment of calculations that rely on idealized geometries and/or that generate structural interpretations based on small energetic differences. One interesting manifestation of the low energetic differences in the 11-vertex systems described here is that only quite minor cluster substituent changes can induce relative stabilization of either the 6,9-bridged "nido form" of the 10-vertex $\{C_2B_8H_9X\}$ ligand (as in structure **1**, Scheme I)[15] or the "arachno form" (as in structure **2**, Scheme I) as the preferred ground-state moiety. Thus for the $\{Pt(PPh_3)_2\}$ and $\{Pt(SEt_2)_2\}$ compounds **1** and **5** the nido form of the the 10-vertex $\{C_2B_8H_9X\}$ ligand is induced, whereas for the $\{Pt(PMe_2Ph)_2\}$ variants **2** and **3** the arachno form is induced. In the species dealt with here, these general changes are electronic rather than steric in origin.

The successive positioning of the 10-vertex $\{C_2B_8H_9X\}$ ligand units of compounds **1** and **2** (or **3**) along the nido $\rightarrow\rightarrow\rightarrow$ arachno continuum is also supported by a comparison of their cluster ^{11}B NMR shielding patterns with those of the conventional 10-vertex nido and arachno models $[6,9\text{-}C_2B_8H_{10}]^{2-}$ and [6,9-$C_2B_8H_{14}$], respectively (Figure 3).[15] It can be seen that the arachno shielding pattern is well mirrored by compound **3**, whereas compound **1** has much more nido character (albeit nearer to the crossover point for the effective inversion of the ^{11}B shielding pattern that is characteristic[19] of a nido $\leftrightarrow$ arachno 10-vertex interconversion).

Acknowledgment. We thank the Royal Society, London, the SERC (U.K.), and Borax Research Limited for support, Dr. J.

(13) Cluster ^{11}B and ^1H NMR properties for compounds **2**, **3**, and **4** (this work, 294–297 K) are ordered as follows: (assignment) $\delta(^{11}B)$/ppm [$\delta(^1H)$/ppm in square brackets]. Compound **2** ($CDCl_3$ solution): (8) +10.6 [+3.90 {$^3J(^{195}Pt\text{–}^1H)$ = 91 Hz}], (9) +1.5 [+3.66 {$^3J(^{195}Pt\text{–}^1H)$ = 103 Hz}], (4,5) −12.0 [+1.51], (6,7) −12.8 [+1.45], (10,11) −26.2(−0.53), (3) (CH) ... [+4.92], (2) (CMe) ... [+3.16 {$^3J(^{195}Pt\text{–}^1H)$ = 26 Hz}]. Compound **3** (CD_2Cl_2 solution): (8,9) −0.8 [+3.50 {$^3J(^{195}Pt\text{–}^1H)$ = 80 Hz}], (4,5,6,7) −10.3 [+1.60], (10,11) −19.9[+0.15], (2,3) (CH) ... [+4.72]. Compound **4** (CD_2Cl_2 solution): (8) +8.6 [+3.87 {$^3J(^{195}Pt\text{–}^1H)$ = 93 Hz}], (9) −3.2 [+3.69 {$^3J(^{195}Pt\text{–}^1H)$ = +103 Hz}], (4,5) and (6,7) −13.3 and −13.3 [+1.83 and +1.54], (10,11) −25.7 [−0.47], (3) (CH) ... [+5.09].

(14) Cluster NMR properties for compounds **1** and **5**. [1,1-$(PPh_3)_2$-1,2,3-$PtC_2B_8H_{10}$] (compound **1**) (data from refs 6 and 7): $\delta(^{11}B)$(4,5,6,7) −5.5, $\delta(^{11}B)$(8,9 and 10,11) −9.0 and −12.0 ppm [1,1-$(SEt_2)_2$-1,2,3-$PtC_2B_8H_{10}$] (compound **5**) (this work, CD_2Cl_2, 294–297 K), ordered as (assignment) $\delta(^{11}B$/ppm) [$\delta(^1H)$/ppm in square brackets]: (8,9) −10.4 [2.59 {$^3J(^{195}Pt\text{–}^1H)$ = 80 Hz}], (4,5,6,7) −5.7 [+2.02], (10,11) −13.3 [+1.15], (2,3)(CH) ... [+3.19 {$^3J(^{195}Pt\text{–}^1H)$ = 34 Hz}].

(15) Note that the numbering conventions are such that the 6,9-positions (carbon) in these nido and arachno 10-vertex clusters become the 2,3-carbon positions in the closed 11-vertex clusters of compounds **1**–**6**.

(16) Schubert, D. M.; Knobler, C. B.; Rees, W. S.; Hawthorne, M. F. *Organometallics* **1987**, *6*, 201–202.

(17) Macgregor, S. A.; Yellowlees, L. J.; Welch, A. J. *Acta Crystallogr., Sect. C* **1990**, *C46*, 551–554 and 1399–1402. Wynd, A. J.; Welch, A. J.; Parish, R. V. *J. Chem. Soc., Dalton Trans.* **1990**, 2185–2193.

(18) Faridoon; Ni Dhubhghaill, O.; Spalding, T. R.; Ferguson, G.; Kaitner, B.; Fontaine, X. L. R.; Kennedy, J. D. *J. Chem. Soc., Dalton Trans.* **1989**, 1657–1668.

(19) Beckett, M. A.; Kennedy, J. D. *J. Chem. Soc., Chem. Commun.* **1983**, 575–576.

B. Farmer, Mr. D. Perryer, and Dr. T. S. Griffin for their helpful cooperation, and Dr. X. L. R. Fontaine for NMR spectroscopy.

Registry No. 1, 75701-67-6; 2, 136629-72-6; 3, 136629-73-7; 4, 136629-74-8; 5, 94100-42-2.

Supplementary Material Available: Tables of data collection parameters, atomic parameters, anisotropic thermal parameters, hydrogen atom parameters, and interatomic distances and angles for 2 and 3 (14 pages); tables of structure factors for 2 and 3 (21 pages). Ordering information is given on any current masthead page.

School of Chemistry
University of Leeds
Leeds LS2 9JT, England

John D. Kennedy*
Mark Thornton-Pett

Institute of Inorganic Chemistry
Czechoslovak Academy of Sciences
25068 Řež u Prahy, Czechoslovakia

Bohumil Štíbr*
Tomáš Jelínek

Received March 7, 1991

Thermodynamic Nucleic Base Specificity in Nucleotide–Metallointercalator Association. Structure–Stability Relationship Showing Significant Contribution of the Amino Group to Aromatic Ring Stacking

Intercalation of planar compounds into base pairs of DNA greatly influences the properties of DNA and is thought to be the first step in mutagenesis.[1] Platinum(II) and other metal complexes with heteroaromatic rings (L) such as bpy and phen interact with DNA and nucleotides by stacking interactions with the base pairs.[2,3] The positive charge of the Pt(II) complexes probably contribute to intercalation through the initial electrostatic bonding with the phosphate oxygens of DNA.[4] Our previous circular dichroism (CD) and ^{1}H NMR spectral studies on the intercalation of the platinum(II) intercalators Pt(L)(en) (L = bpy, phen,

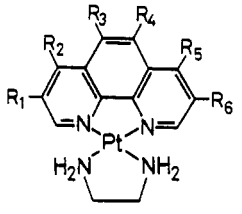

Pt(L)(en)

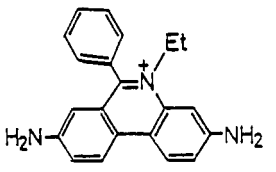

ethidium

L = phen ($R_1=R_2=R_3=R_4=R_5=R_6=H$)
Me_2phen ($R_1=R_2=R_5=R_6=H$, $R_3=R_4=CH_3$)
Me_4phen ($R_1=R_2=R_5=R_6=CH_3$, $R_3=R_4=H$)

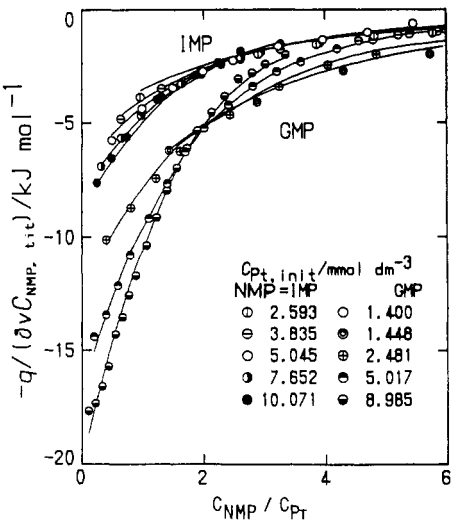

Figure 1. Calorimetric titration curves for Pt(phen)(en)–GMP and –IMP systems at pH 7–8 and 25 °C (I = 0.1 M (NaCl)). Key: q, heat liberated per unit volume of titer; C_{NMP}, concentration of NMP; C_{Pt}, concentration of Pt(L)(en).

Table I. Stability Constants, log β_1, and Thermodynamic Quantities, $\Delta H_1°$ and $\Delta S_1°$, for 1:1 Intercalator–NMP Adduct Formation at 25 °C and pH 7–8 (I = 0.1 or 0.2 M (NaCl))[a]

intercalator	NMP	I, M	log β_1[c]	$\Delta H_1°$/kJ mol^{-1}	$\Delta S_1°$/J mol^{-1} K^{-1}
Pt(phen)(en)	IMP	0.1	2.34 (0.08)	−11.9 (0.9)	5
	GMP[b]	0.1	2.49 (0.03)	−26.2 (0.8)	−40
	AMP[b]	0.1	2.51 (0.03)	−25.6 (0.8)	−38
	CMP	0.1	2.17 (0.08)	−6.5 (0.5)	20
ethidium	IMP	0.2	1.86 (0.14)	−4.0 (0.5)	22
	GMP	0.2	2.01 (0.04)	−9.1 (0.3)	8
	AMP	0.2	1.92 (0.13)	−9.3 (1.1)	6

[a] Values in parentheses denote estimated standard deviations. [b] Taken from ref 8. [c] Units of β_1 are mol^{-1} dm^3.

Me_4phen) with several mononucleotides (NMP) as fundamental constituents of nucleic acids have shown that the intercalators have an intrinsic tendency to stack with nucleotides and nucleosides in dilute aqueous solution.[5] In addition to the structural studies on related metallointercalator–nucleotide adducts[6] the X-ray crystal structure analysis of an adduct [Pt(bpy)(en)]·AMP·10H_2O also revealed the stacking between bpy and the adenine ring of AMP,[7] supporting the conclusion from the spectra. As an extension of these studies[5,7,8] we investigated adduct formation between Pt(L)(en) and NMP containing purine and pyrimidine bases with or without an amino group. An important effect of the nucleic base amino group, which is involved in the hydrogen bonds between base pairs in DNA, is that it alters the electron density of the base,[9] and this is potentially related to the base specificity of intercalators and other reagents that have affinity for nucleic acids. We here report the systematic thermodynamic characterization of Pt(L)(en)–NMP adduct formation and the NMR spectral evidence that the amino group attached to the nucleic bases makes a substantial contribution to the stacking

(1) (a) Guschlbauer, W., Saenger, W., Eds. *DNA-Ligand Interactions*; Plenum: New York, 1987. (b) Saenger, W. *Principles of Nucleic Acid Structure*; Springer Verlag: New York, 1984. (c) Waring, M. J. *Annu. Rev. Biochem.* **1981**, *50*, 159–192.
(2) (a) Lippard, S. J. *Acc. Chem. Res.* **1978**, *11*, 211–217. (b) Barton, J. K.; Lippard, S. J. *Nucleic Acid-Metal Ion Interactions*; Spiro, T. G., Ed.; Wiley Interscience: New York, 1980; pp 31–113. (c) Sandquist, W. I.; Lippard, S. J. *Coord. Chem. Rev.* **1990**, *100*, 293–322. (d) Naumann, C. F.; Sigel, H. *J. Am. Chem. Soc.* **1974**, *96*, 2750–2756. (e) Massoud, S. S.; Sigel, H. *Inorg. Chim. Acta* **1989**, *159*, 243–252. (f) Massoud, S. S.; Tribolet, R.; Sigel, H. *Eur. J. Biochem.* **1990**, *187*, 387–393. (g) Carter, M. T.; Rodriguez, M.; Bard, A. J. *J. Am. Chem. Soc.* **1989**, *111*, 8901–8911.
(3) The following abbreviations were used: bpy, 2,2′-bipyridine; phen, 1,10-phenanthroline; Me_2phen, 5,6-dimethyl-1,10-phenanthroline; Me_4phen, 3,4,7,8-tetramethyl-1,10-phenanthroline; en, ethylenediamine; AMP, adenosine 5′-monophosphate; GMP, guanosine 5′-monophosphate; CMP, cytidine 5′-monophosphate; UMP, uridine 5′-monophosphate; IMP, inosine 5′-monophosphate.
(4) (a) Watson, J. D.; Hopkins, N. H.; Roberts, J. W.; Steitz, J. A.; Weiner, A. M. *Molecular Biology of the Gene*, 4th ed.; Benjamin/Cumming: Menlo Park, CA, 1987. (b) Kumar, C. V.; Barton, J. K.; Turro, N. J. *J. Am. Chem. Soc.* **1985**, *107*, 5518–5523.
(5) Yamauchi, O.; Odani, A.; Shimata, R.; Kosaka, Y. *Inorg. Chem.* **1986**, *25*, 3337–3339.
(6) (a) Wong, Y.-S.; Lippard, S. J. *J. Chem. Soc., Chem. Commun.* **1977**, 824–825. (b) Wang, A. H. J.; Nathans, J.; van der Marel, G.; van Boom, J. H. *Nature* **1978**, *276*, 471–474. (c) Vijay-Kumar, S.; Sakore, T. D.; Sobell, H. M. *Nucleic Acids Res.* **1984**, *12*, 3649–3657. (d) Vijay-Kumar, S.; Sakore, T. D.; Sobell, H. M. *Biomol. Struct. Dyn.* **1984**, *2*, 333–344. (e) Colquhoun, H. M.; Goodings, E. P.; Maud, J. M.; Stoddart, J. F.; Wolstenholme, J. B. *J. Chem. Soc., Perkin Trans. 2* **1985**, 607–624.
(7) Masuda, H.; Yamauchi, O. *Inorg. Chim. Acta* **1987**, *136*, L29.
(8) Yamauchi, O.; Odani, A.; Shimata, R.; Ishiguro, S. *Recl. Trav. Chim. Pays-Bas* **1987**, *106*, 196–197.
(9) Berthod, H.; Giessner-Prettre, C.; Pullman, A. *Theor. Chim. Acta* **1966**, *5*, 53–68.

0020-1669/91/1330-4484$02.50/0